UNIVERSITEIT
AMSTERDAM

VU Research Portal

Slice imaging of the quantum state-to-state cross section for photodissociation of state-selected rovibrational bending states of OCS (v2=0,1,2/JlM)+hnu-->CO(J)+S(1D2)

Lipciuc, ML; Janssen, M.H.M.

document version
Publisher's PDF, also known as Version of record

Link to publication in VU Research Portal

Download date: 23. May. 2021

Slice imaging of the quantum state-to-state cross section for photodissociation of state-selected rovibrational bending states of OCS $(v_2=0,1,2|JlM)+h\nu \rightarrow CO(J)+S(^1D_2)$

M. Laura Lipciuc and Maurice H. M. Janssen[a)]
*Laser Centre, Vrije Universiteit, de Boelelaan 1083, 1081 HV Amsterdam, The Netherlands and
Department of Chemistry, Vrije Universiteit, de Boelelaan 1083, 1081 HV Amsterdam, The Netherlands*

Using hexapole quantum state-selection of OCS $(v_2=0,1,2|JlM)$ and high-resolution slice imaging of quantum state-selected CO(J), the state-to-state cross section OCS $(v_2=0,1,2|JlM)+h\nu \rightarrow CO(J)+S(^1D_2)$ was measured for bending states up to $v_2=2$. The population density of the state-selected OCS $(v_2=0,1,2|JlM)$ in the molecular beam was obtained by resonantly enhanced multiphoton ionization of OCS and comparison with room temperature bulk gas. A strong increase of the cross section with increasing bending state is observed for CO(J) in the high J region, $J=60-67$. Integrating over all J states the authors find $\sigma(v_2=0):\sigma(v_2=1):\sigma(v_2=2) =1.0:7.0:15.0$. A quantitative comparison is made with the dependence of the transition dipole moment function on the bending angle. © *2007 American Institute of Physics*. [DOI: 10.1063/1.2737450]

I. INTRODUCTION

Quantum state-to-state measurements provide the most accurate experimental data for comparison with *ab initio* quantum calculations of the differential cross section of a single state-to-state photodissociation channel.[1] The photodissociation of carbonyl sulfide (OCS) has received a lot of attention in the last 20 years and it has become a benchmark system for dynamical aspects such as the breakdown of axial recoil in molecular photodissociation.[2] The photodissociation of OCS has been investigated[3–17] extensively in the wavelength region of $222-248$ nm which is around the maximum of the absorption spectrum.[18]

The OCS molecule is a good system for studying the dependence of the transition dipole moment on the initial molecular geometry, in particular the effect of the bending excitation on the photodissociation dynamics. The OCS$(X\,^1\Sigma^+)$ molecule in the electronic ground state is a linear molecule. The dissociation at wavelengths around 230 nm leads to the production of S(95% $^1D_2$, 5% ^3P) and CO$(X\,^1\Sigma^+)$ photofragments which have little vibrational excitation but are highly rotationally excited.[5] The dissociation takes place through excitation to the $1\,^1\Delta$ and $1\,^1\Sigma^-$ electronic states which are bent. Away from linear geometry the $1\,^1\Delta$ excited state splits into the $2\,^1A'$ and $2\,^1A''$ states and the $1\,^1\Sigma^-$ becomes the $1\,^1A''$ state. At 230 nm only the $2\,^1A'(^1\Delta)$ and $1\,^1A''(^1\Sigma^-)$ are accessed. The bimodal structure observed for the CO(J) rotational distribution and for the translational energy of the S$(^1D_2)$ was attributed by Suzuki *et al.*[7] to the fact that dissociation on the $2\,^1A'(^1\Delta)$ excited state takes place through both adiabatic and nonadiabatic transitions. The latter process allows exit channel tran-

sitions from the initially $2\,^1A'(^1\Delta)$ excited state to the $1\,^1A'(^1\Sigma^+)$ ground state which is believed to cause a splitting of the initial wave packet. The probability of this nonadiabatic transition was found to be 0.35.[7]

Electronic transitions from the ground state $X\,^1\Sigma^+$ to the excited states $^1\Delta$ and $^1\Sigma^-$ are forbidden in the linear equilibrium geometry, but they are allowed in the bent geometry (C_s). The bending excitation plays an important role in the OCS dissociation dynamics. As suggested by Sugita *et al.*[9] the bending excitation in OCS increases the Franck-Condon overlap between the ground electronic state and the excited states at the lower excitation energy region; it reduces the energy difference between the energy surfaces and enhances the potential curve crossing. The transition dipole moment also increases with the bending angle and it increases more steeply for the $2\,^1A' \leftarrow 1\,^1A'$ transition than for the $1\,^1A'' \leftarrow 1\,^1A'$ transition.[7] It was concluded from the analysis of the β parameter that the transition probability to the $2\,^1A'$ state for ground state OCS$(v_2=0)$ is smaller than vibrationally excited OCS$(v_2=1)$.[19]

The effect of the vibrational bending excitation of OCS on the photodissociation dynamics in a molecular beam was investigated around 230 nm (Refs. 9, 11, 15, and 19) and 288 nm.[14] From the detection of the S$(^1D_2)$ fragments from OCS photolysis at 288 nm, Kim *et al.*[14] reported photodissociation from excited bending levels up to $v_2=4$ in the OCS parent molecule. They also reported that the absorption cross section for bent-excited OCS parent molecule to the $1\,^1A''(^1\Sigma^-)$ surface is greatly enhanced relative to the OCS parent molecule in the ground vibrational state. However, in the absence of quantitative information on the initial population distribution over the vibrational bending levels, no quantitative information on the increase of the cross section with bending level could be extracted.

The effect of bending excitation on the photodissociation

---

a)Author to whom correspondence should be addressed. Electronic mail: mhmj@chem.vu.nl

of the similar linear molecule N_2O has also been studied especially in the context of mass independent fractionation processes in atmospheric N_2O.[20,21] Recently, Kawamata *et al.*[22] reported new quantitative results on the experimental cross section for photodissociation of excited bending levels $v_2 = 0, 1, 2$ of N_2O.

In this paper we report quantitative results for the state-to-state cross section of OCS from bending levels $v_2 = 0, 1, 2$. We performed high-resolution slice imaging experiments on state-selected molecules. We calibrated the population density of $OCS(v_2 = 0, 1, 2 | J)$ parent molecules using a $(2+1)$ resonantly enhanced multiphoton ionization (REMPI) detection on parent molecules. We have measured the quantum state-to-state cross section for single rotational quantum states of the final $CO(J = 60 - 67)$ fragment. In Sec. II we present the experimental technique and in Sec. III we present and discuss the experimental results.

II. EXPERIMENT

The experimental setup has been described in detail elsewhere.[11,23–25] Here we give only a brief description of the experimental conditions. A mixture of 20% OCS seeded in Ar is supersonically expanded through a pulsed nozzle and skimmed before it enters a buffer chamber which contains a beamstop. The beamstop (a metal sphere of 1 mm in diameter) is positioned on the molecular beam axis, 10 cm before the hexapole. It is used to enhance the selectivity of the hexapole because it blocks the molecules traveling along the center axis where the electric field is weak or zero. The hexapole focuses the OCS molecules through the first and second order Stark effect onto a collimator, a 1 mm diameter hole in the repeller plate of the ion optics. The state-selected OCS molecules enter the imaging chamber which contains an electrostatic ion lens: three cylindrical electrodes, the repeller, extractor, and an extra electrode.[25,26] In between the repeller and the extractor plate the molecular beam is intersected, at right angle, by a linearly polarized photolysis laser. After passing through a field-free region for mass separation, the CO and OCS ions reach the position sensitive detector [micro-channel-plate (MCP)/phosphor screen/charge coupled device (CCD)]. We use slice imaging[27–29] to measure the three-dimensional velocity distribution. In particular we developed a fast homebuilt high-voltage switch to gate the MCP detector. The light from the phosphor screen is collected simultaneously by a photomultiplier and a large frame (2048 by 2048 pixels) CCD camera. We use an on-the-fly centroiding algorithm to read out the data recorded with the CCD camera.[25,26]

For the experiments detecting the CO fragment we used a 230 nm photon for both the photolysis of OCS and the ionization of the $CO(X\,^1\Sigma^+; v=0 | J)$ photofragment, using a $(2+1)$ REMPI scheme via the two-photon Q-band transition to the $B\,^1\Sigma^+$ resonant intermediate state.[6,12] For the experiments detecting the OCS parent molecule we used a 282 nm photon to ionize the OCS molecules by $(2+1)$ REMPI via the $(^2\Pi_{3/2})4p\pi\,^3\Delta \leftarrow \leftarrow \widetilde{X}\,^1\Sigma^+ 0_0^0$, 2_1^1, and 2_2^2 vibronic transitions.[30]
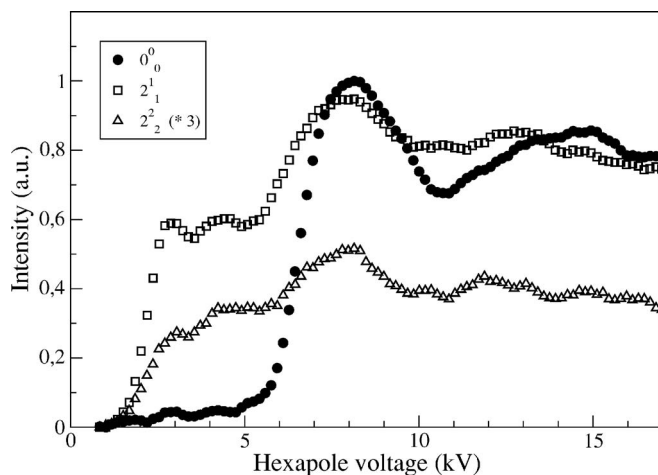

FIG. 1. Hexapole focusing spectra of OCS (20% in Ar) detected by parent molecule ionization through $^3\Delta \leftarrow \leftarrow \widetilde{X}\,^1\Sigma^+$ 0_0^0 (solid circle), 2_1^1 (open square), and 2_2^2 (open triangle) vibronic transitions. Each peak in all three spectra corresponds to an individual rotational state of the OCS parent molecule or to a convolution of several rotational states (see Fig. 3). The intensity of the spectrum detected through the 2_2^2 transition of OCS was multiplied by a factor of 3 for better viewing. The hexapole voltage is the voltage difference between the positive and the negative rods.

III. RESULTS AND DISCUSSION

A. Hexapole focusing

In Fig. 1 we present three hexapole focusing spectra for a molecular beam of 20% OCS seeded in Ar. The OCS molecules were detected through REMPI using three vibronic transitions, 0_0^0 at 70 881 cm^{-1}, 2_1^1 at 70 805 cm^{-1}, and 2_2^2 at 70 741 cm^{-1}, belonging to the $^3\Delta \leftarrow \leftarrow \widetilde{X}\,^1\Sigma^+$ electronic transition.[30] The OCS molecules are focused and state-selected through first order Stark effect when the bending vibration is excited, $v_2 = 1, 2$. If the OCS molecules are in the ground vibrational state the focusing is achieved via the second order Stark effect.[31] Each focusing spectrum in Fig. 1 contains various peaks representing the position where different OCS rotational states focus. By choosing a certain value for the hexapole voltage we can select the desired rotational state of the OCS molecule.

In order to simulate the focusing spectra and the trajectories of the OCS molecules through our machine we need to include the molecular beam velocity distribution. We determined the velocity distribution by scanning the delay between the nozzle trigger and the laser trigger, see Fig. 2. We need to remark here that the typical opening time of the valve is about 180 μs and this is not negligible compared to the measured full width at half maximum (FWHM) of the velocity distribution of 650 μs. This means that our extracted translational temperature is an upper limit and the real temperature may be somewhat lower. By fitting a Gaussian function we determine the FWHM and the central velocity for the beam of OCS seeded in Ar. The central velocity of the molecular beam is found to be 540 m/s. We determined the translational temperature $T_\parallel$ from the relation $T_\parallel = m(\Delta v_\parallel)^2 / 2k_B$, where the width in the longitudinal velocity $\Delta v_\parallel$ can be related to the FWHM as follows: $\Delta v_\parallel = \text{FWHM}/2\sqrt{\ln 2}$. For state-selected $OCS(JlM = 100)$ we find a translational temperature of 17 K. We use these values for
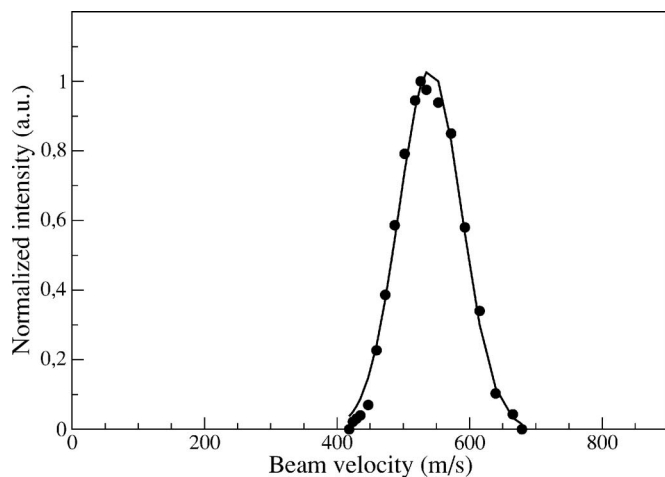
FIG. 2. Molecular beam profile. We measured the intensity of the OCS ions as we varied the time delay between the molecular beam and the laser beam. From the width of the gas pulse we determine the translational temperature of the molecular beam.

the molecular beam speed and translational temperature in the simulated spectra shown in Fig. 3. The hexapole focusing simulation program of Anderson was used.[32] In the upper panel of Fig. 3 the measured and the calculated spectra for OCS molecules in the ground vibrational state are shown. Within the range of $0-20$ kV there are two peaks in the focusing spectrum when detecting ground state OCS, a first peak near 8 kV, where OCS$(JlM=100)$ is focused, and a
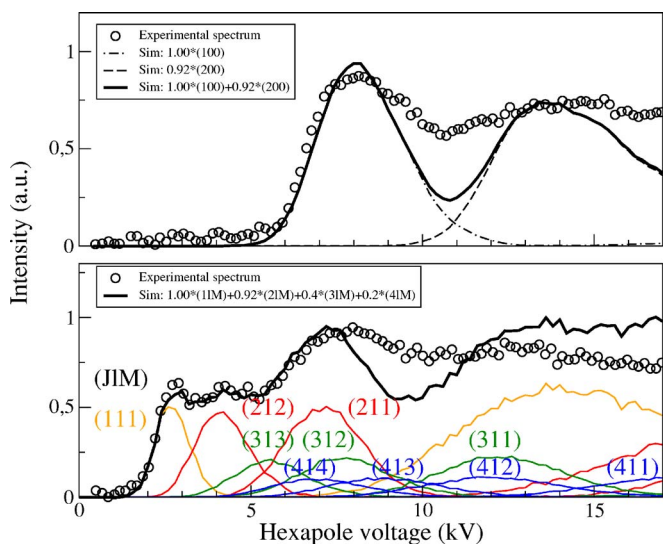

FIG. 3. (Color online) Simulated and measured hexapole focusing spectra of OCS$(v_2=0,1)$. Upper panel: the measured hexapole spectrum (open circles) for ground state OCS$(v_2=0)$ shows two peaks which can be assigned to the focusing, by second order Stark effect, of OCS$(v_2=0|JlM=100)$ around 7.8 kV and OCS$(v_2=0|JlM=200)$ around 13.5 kV. Individual rotational states of the OCS molecule are simulated: $(JlM)=(100)$ (dashed line) and (200) (dot-dashed line). The solid line gives the sum of the two rotational states with a relative weight of the population of $n(100):n(200)=1:0.92$. Lower panel: the measured hexapole spectrum (open circle) and the simulated spectrum (solid line) for OCS$(v_2=1|JlM)$ molecules with one quantum of vibrational excitation. The focusing curves of individual (JlM) rotational states are shown by the colored curves and are labeled by the quantum numbers (JlM). The simulations were run for a molecular beam with a central translational velocity of 540 m/s and a translational temperature of 17 K.

second peak near 13.5 kV, where OCS$(JlM=200)$ is focused. The second peak is slightly lower in intensity and we find a best fit when we use a population ratio of $n(100):n(200)=1:0.92$. For the OCS $(v_2=0|JlM=100$ and 200) molecules the measurements and the simulation are in good agreement, with the exception that in the simulated spectrum the peaks are better separated.

The focusing spectra for the OCS molecules with one quanta excited in the bending vibration are shown in the lower panel of Fig. 3. For OCS$(v_2=1|JlM)$ molecules the measurements agree with the calculation especially in the region of lower focusing voltages. All measurements presented below were done with the hexapole set at 7.8 kV. At this voltage the OCS molecules which were focused in the interaction region are OCS$(v_2=0|JlM=100)$ and OCS$(v_2=1,2|JlM=211,312,321,414,413)$. Notice that the high $(J=4)$ rotational states for the OCS molecules with the bending vibration excited have low population, so it is fair to say that at this hexapole voltage we mainly focus OCS molecules in the (211), (312), and (321) rotational states.

B. Calibration of population density OCS($v_2=0,1,2$)

To determine the population density of OCS$(v_2=0,1,2)$ in a hexapole focused molecular beam, we performed REMPI detection at room temperature of OCS bulk gas in the same imaging chamber. Assuming a Boltzmann distribution of the population density for bulk gas at $T=293$ K, the thermal populations for excited vibrational bending states relative to the ground state of OCS parent molecules can be calculated as $n(v_2=1)/n(v_2=0)=0.1555$ and $n(v_2=2)/n(v_2=0)=0.01\,208$. The vibrational energies of OCS parent molecules with one and two quanta excitations of the bending vibration are 520.41 and 1041 cm^{-1}.[33] To determine the efficiency of laser detection of OCS molecules, which are in the vibrational ground state relative to the vibrationally excited states, we performed an experiment using bulk gas. We detect OCS parent molecules in the ground vibrational state and in the vibrationally excited states through the 0^0_0, 2^1_1, and 2^2_2 vibronic transitions. When the laser was tuned to detect the OCS through the 0^0_0 vibronic transition we measured the $n_{v_2=0}I_{\text{laser}0^0_0}$ product, which represents the number of OCS molecules in the ground vibrational state multiplied by the laser detection efficiency for OCS$(v_2=0)$ molecules. When the laser was tuned to detect OCS through the 2^1_1 and 2^2_2 vibronic transitions we measured the $n_{v_2=1}I_{\text{laser}2^1_1}$ and $n_{v_2=2}I_{\text{laser}2^2_2}$ products, which represent the number of OCS molecules in the $v_2=1,2$ vibrational states multiplied by the laser efficiency in detecting the corresponding molecules. We measured the following relative REMPI signals for bulk gas $n_{v_2=0}I_{\text{laser}0^0_0}=1$, $n_{v_2=1}I_{\text{laser}2^1_1}=0.5$, and $n_{v_2=2}I_{\text{laser}2^2_2}=0.14$. With these measured signals and the known Boltzmann population, we determine the relative laser detection efficiencies of OCS molecules in the vibrationally excited states relative to those in the ground vibrational state $I_{\text{laser}2^1_1}/I_{\text{laser}0^0_0}=0.5(n_{v_2=0}/n_{v_2=1})=3.22$ and $I_{\text{laser}2^2_2}/I_{\text{laser}0^0_0}=0.14(n_{v_2=0}/n_{v_2=2})=11.6$.

As can be seen in Figs. 1 and 3 when the hexapole is set at a voltage around 7.8 kV, the hexapole focuses

$OCS(v_2=0|JlM=100)$, $OCS(v_2=1|JlM=211,312)$,   and $OCS(v_2=2|JlM=321)$ molecules in the interaction region. With the hexapole set at this fixed hexapole voltage we tune the laser wavelength in order to detect the $OCS(v_2=0)$ molecules through the 0_0^0 vibronic transition, $OCS(v_2=1)$ molecules through the 2_1^1 vibronic transition and $OCS(v_2=2)$ molecules through the 2_2^2 vibronic transition. The measured signals $n_{v_2=i}I_{\text{laser}i}i_i^i$ are 1.00, 0.976, and 0.172 for $v_2=0,1,2$, respectively. These measurements, together with the calibration of the relative laser detection efficiencies for OCS molecules in the vibrationally excited states relative to those in the ground vibrational state, allow us to determine the density of rovibrationally state-selected OCS molecules focused by the hexapole in the interaction region. Relative to the population density of focused $OCS(v_2=0|JlM=100)$ molecules $n(v_2=0|JlM=100)=1$, we obtain the density of $OCS(v_2=1|JlM=211,312)$ molecules $n(v_2=1|JlM=211,312)=0.294$ and the density of $OCS(v_2=2|JlM=321)$ molecules $n(v_2=2|JlM=321)=1.48\times10^{-2}$.

C. State-to-state cross section

In Fig. 4 we present three raw data images of CO $(v=0|J=60,63,$ and 67) from photolysis of $OCS(v_2=0,1,2)$, with the hexapole voltage set at 7.8 kV. The same laser pulse was used to photodissociate the OCS molecules and to resonantly detect the CO(J) photofragments. Three rings are visible in all three images. The first ring at the shortest radius (i.e., with lowest kinetic energy) originates from the dissociation of ground state $OCS(v_2=0|JlM=100)$. The second ring originates from the dissociation of $OCS(v_2=1|JlM=211,312)$ and the third ring correlates with the photolysis of $OCS(v_2=2|JlM=321)$. The energy separation between the rings is given by the difference in the available energy from the photolysis of OCS parent molecules in the vibrational ground state, $v_2=0$, or in vibrational excited states, $v_2=1,2$. We use these energies to calibrate internally the velocity axis in the images.[17]

To obtain the velocity distribution of the images in Fig. 4, we integrate over the angular range the intensity of each ring at a constant radius ρ by multiplying the ion events at each pixel by $\rho\sin\theta$, where θ is the angle between the recoil velocity and the vertical direction of the polarization of the photolysis laser. The velocity distributions for the three representative J values of Fig. 4 are shown in Fig. 5. Three peaks, with different intensities, are seen in each spectrum corresponding to the three rings seen in the images.

To obtain the state-to-state cross section we integrate the intensity of the rings of the CO(J) images, for $J=60$ till $J=67$, and divide the outcome by the population of the corresponding $OCS(v_2=0,1,2|JlM)$ state, as obtained from the measurement described in Sec. III B. The results are given graphically in Fig. 6 and numerically in Table I. As can be seen in Table I the photodissociation cross section changes with the CO fragment rotational state. The cross section for the excited OCS molecule $\sigma(v_2=1)$ is greater than the cross section of the vibrationless OCS molecule $\sigma(v_2=0)$. The ratio $\sigma(v_2=1)/\sigma(v_2=0)$ varies from ~3.5 for $J_{CO}=62$ to ~23 for $J_{CO}=64$. The photodissociation cross section for the ex-
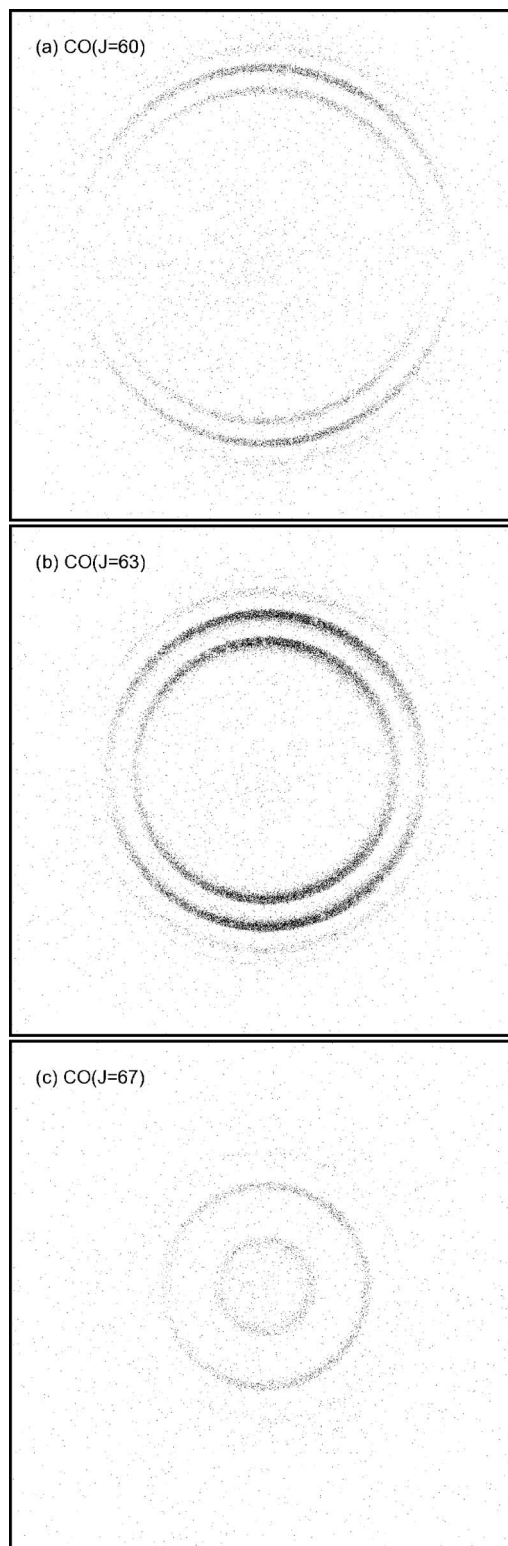

FIG. 4. Slice images of CO(J) measured in one laser experiment with the laser frequency tuned to three different CO(J) levels, (a) $J=60$, (b) $J=63$, and (c) $J=67$. The images shown are a cut of 1050 by 1050 real pixels of the 2048 by 2048 CCD pixels. The total number of ion events in these images are (a) 8411, (b) 35310, and (c) 3268. Clearly visible are three rings in each image and the diameter of the rings decrease with increasing rotational state.

citation of the bending motion with two quanta in OCS molecules $\sigma(v_2=2)$ is even larger. The ratio $\sigma(v_2=2)/\sigma(v_2=0)$ varies from ~7.6 for $J_{CO}=62$ to ~54 for $J_{CO}=66$.

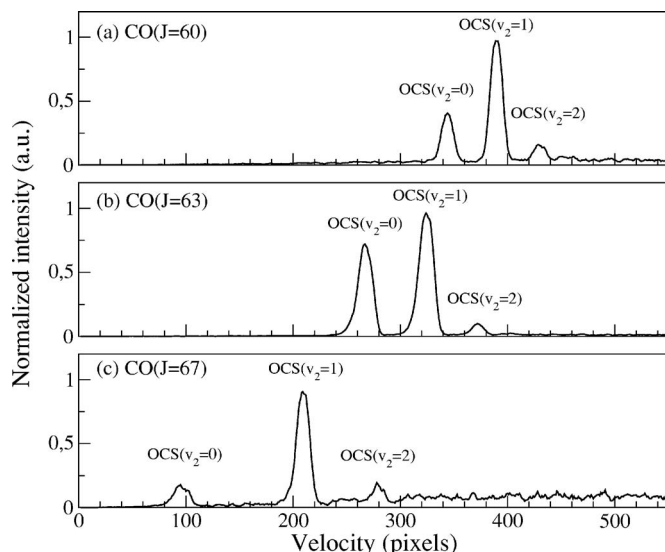These values for the photodissociation cross section can

FIG. 5. The radial velocity distribution (in pixel units) obtained from the corresponding images in Fig. 4 are presented in panel (a) for $J=60$, panel (b) for $J=63$, and panel (c) for $J=67$. The labels $v_2=0,1,2$ at the various peaks indicate the initial number of quanta excited in the v_2 bending vibration of the OCS molecule.

be compared to the results reported by Katayanagi and Suzuki.[19] In this paper the authors assume a room temperature Boltzmann distribution of the vibrational state population and they report that the cross section for $v_2=1$ is about seven times greater than $v_2=0$. The photodissociation cross section at 288 nm of hot bands from bending excited states of OCS are reported by Kim et al.[14] They found that the photodissociation cross section is greatly enhanced by bending excitation in OCS, with a factor of 44 for $\sigma(v_2=2)$ compared to $\sigma(v_2=1)$ and a factor of 1.8×10^3 for the $\sigma(v_2=4)$ compared to $\sigma(v_2=1)$. From our measurements we see that the photodissociation cross section $\sigma(v_2=0)$ peaks at $J_{CO}=63$, while the cross section for the bending excitation $\sigma(v_2=1)$ and $\sigma(v_2=2)$ peaks at $J_{CO}=64$. This behavior is similar to the small change reported for the rotational distribution of N_2 from the photolysis of the isoelectronic N_2O molecule. It is observed in the wave packet calculations by
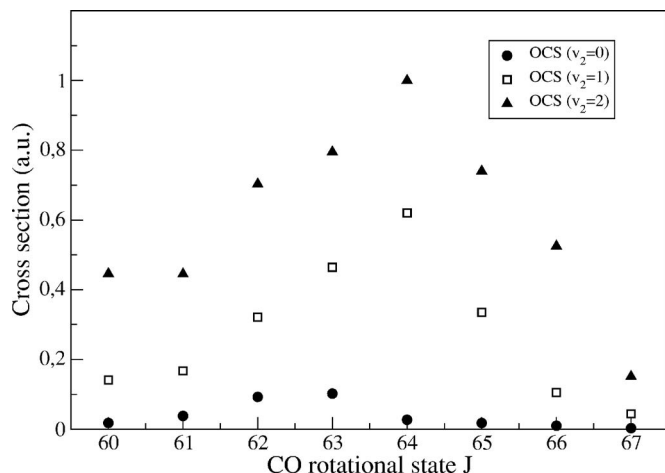

FIG. 6. The state-to-state OCS photodissociation cross section at 230 nm as a function of the CO rotational state and the initial bending state OCS($v_2=0,1,2$).

TABLE I. The state-to-state OCS photodissociation cross section at 230 nm.

J_{CO}	$\sigma\,(v_2=0)$	$\sigma\,(v_2=1)$	$\sigma\,(v_2=2)$
60	0.02	0.14	0.44
61	0.04	0.17	0.44
62	0.09	0.32	0.70
63	0.10	0.46	0.80
64	0.03	0.62	1.00
65	0.02	0.34	0.74
66	0.01	0.11	0.53
67	0.003	0.04	0.15
Σ_J	0.31	2.2	4.7

Daud et al.[34] that one quantum of bending excitation shifts the peak of the N_2 rotational distribution by one quantum in J.

D. The dependence of the transition dipole moment on bending angle

The enhancement of the photodissociation cross section with the bending excitation in the OCS (v_2) parent molecule has been attributed to the strong increase of the transition dipole moment with bending angle. Suzuki et al.[7] have calculated the transition dipole moment function and these calculations indicate that there is a strong increase with increasing bending angle. To compare our experimental results for the state-to-state cross section we integrated the cross section as given in Table I over all J states in this high J region; the result is also given in the last row of Table I. We find that the integrated cross section $\sigma(v_2=0):\sigma(v_2=1):\sigma(v_2=2)$ $=1.0:7.0:15.0$. We have made a quantitative comparison by integrating the bending state wave function probability over the transition dipole moment function. As was discussed by Suzuki et al.[7] the photon excitation leading to CO(J) with high J is due to the parallel component of the transition dipole moment. The ab initio values were calculated at angular bending angles of 0°, 10°, and 20° (Ref. 35), and we fitted a polynomial to these ab initio values. We find for the total parallel component, $|\bar{\mu}_\parallel(\theta)|=\sqrt{\mu_x^2+\mu_z^2}=a_1\theta+a_2\theta^2$, with $a_1=0.6616$ and $a_2=1.2392$, with the Jacobi bending angle θ in radians. Using the two-dimensional bending wave functions for linear molecules[36] we calculate $\langle\mu_\parallel\rangle_i=\int|\bar{\mu}_\parallel(\theta)|\Psi_i\Psi_i^*(\theta)\sin(\theta)d\theta$ for each bending wave function with $i=0,1,2$ quanta of vibrational excitation. We find $\langle\mu_\parallel\rangle_0:\langle\mu_\parallel\rangle_1:\langle\mu_\parallel\rangle_2=1.0:3.2:4.2$. This increase of the average transition dipole moment with bending wave function qualitatively agrees with the observed increase in cross section. However, the measured increase is stronger than the calculated transition dipole moment. This quantitative difference may be due to the neglect of the explicit inclusion of the excited state wave function, or an underestimate of the increase of the ab initio transition dipole moment function with bending angle. Improved ab initio calculations are needed to compare with experimental results.

IV. CONCLUSIONS

We report the quantum state-to-state photodissociation cross section of $OCS(v_2=0,1,2|J)$ near 230 nm. Hexapole state selection is used to rovibrationally quantum state select the initial OCS parent molecule. High-resolution images of $CO(X^1\Sigma^+; v=0|J=60-67)$ are measured by slice imaging and on-the-fly centroiding. We observe that the vibrational bending excitation of OCS strongly enhances the photodissociation cross section. The cross section also varies with the final CO rotational state. For a single J channel we find the maximum cross section for $OCS(v_2=2)\to CO(J=64)$, which is a factor of 1.6 times larger than $OCS(v_2=1)\to CO(J=64)$ and about 33 times larger than $OCS(v_2=0)\to CO(J=64)$. Integrating over all J states (60–67) in the high J region, we find $\sigma(v_2=0):\sigma(v_2=1):\sigma(v_2=2)=1.0:7.0:15.0$.

[1] R. Schinke, *Photodissociation Dynamics* (Cambridge University Press, Cambridge, 1995).
[2] T. P. Rakitzis, A. J. van den Brom, and M. H. M. Janssen, Science **303**, 1852 (2004).
[3] G. E. Hall, N. Sivakumar, P. L. Houston, and I. Burak, Phys. Rev. Lett. **56**, 1671 (1986).
[4] N. Sivakumar, G. E. Hall, P. L. Houston, J. W. Hepburn, and I. Burak, J. Chem. Phys. **88**, 3692 (1988).
[5] G. Nan, I. Burak, and P. L. Houston, Chem. Phys. Lett. **209**, 383 (1993).
[6] Y. Sato, Y. Matsumi, M. Kawasaki, K. Tsukiyama, and R. Bersohn, J. Phys. Chem. **99**, 16307 (1995).
[7] T. Suzuki, H. Katayanagi, S. Nanbu, and M. Aoyagi, J. Chem. Phys. **109**, 5778 (1998).
[8] Z. H. Kim, A. J. Alexander, and R. N. Zare, J. Phys. Chem. A **103**, 10144 (1999).
[9] A. Sugita, M. Mashino, M. Kawasaki, Y. Matsumi, R. Bersohn, G. Trott-Kriegeskorte, and K.-H. Gericke, J. Chem. Phys. **112**, 7095 (2000).
[10] T. P. Rakitzis, P. C. Samartzis, and T. N. Kitsopoulos, Phys. Rev. Lett. **87**, 123001 (2001).
[11] A. J. van den Brom, T. P. Rakitzis, J. van Heyst, T. N. Kitsopoulos, S. R. Jezowski, and M. H. M. Janssen, J. Chem. Phys. **117**, 4255 (2002).
[12] A. M. Rijs, E. H. G. Backus, C. A. de Lange, M. H. M. Janssen, N. P. C. Westwood, K. Wang, and V. McKoy, J. Chem. Phys. **116**, 2776 (2002).
[13] A. J. van den Brom, T. P. Rakitzis, and M. H. M. Janssen, J. Chem. Phys. **121**, 11645 (2004).
[14] M. Kim, W. Li, S. K. Lee, and A. G. Suits, Can. J. Chem. **82**, 880 (2004).
[15] A. J. van den Brom, T. P. Rakitzis, and M. H. M. Janssen, J. Chem. Phys. **123**, 164313 (2005).
[16] A. J. van den Brom, T. P. Rakitzis, and M. H. M. Janssen, Phys. Scr. **73**, C83 (2006).
[17] M. L. Lipciuc and M. H. M. Janssen, Phys. Chem. Chem. Phys. **8**, 3007 (2006).
[18] J. W. Rabalais, J. M. McDonald, V. Scherr, and S. P. McGlynn, Chem. Rev. (Washington, D.C.) **71**, 73 (1971).
[19] H. Katayanagi and T. Suzuki, Chem. Phys. Lett. **360**, 104 (2002).
[20] M. S. Johnson, G. D. Billing, A. Gruodis, and M. H. M. Janssen, J. Phys. Chem. A **105**, 8672 (2001).
[21] S. Nanbu and M. S. Johnson, J. Phys. Chem. A **108**, 8905 (2004).
[22] H. Kawamata, H. Kohguchi, T. Nishide, and T. Suzuki, J. Chem. Phys. **125**, 133312 (2006).
[23] M. H. M. Janssen, J. W. G. Mastenbroek, and S. Stolte, J. Phys. Chem. A **101**, 7605 (1997).
[24] M. L. Lipciuc, A. J. van den Brom, L. Dinu, and M. H. M. Janssen, Rev. Sci. Instrum. **76**, 123103 (2005).
[25] M. L. Lipciuc, J. B. Buijs, and M. H. M. Janssen, Phys. Chem. Chem. Phys. **8**, 219 (2006).
[26] M. L. Lipciuc, J. B. Buijs, and M. H. M. Janssen, Rev. Sci. Instrum. (submitted).
[27] C. R. Gebhardt, T. P. Rakitzis, P. C. Samartzis, V. Ladopoulos, and T. N. Kitsopoulos, Rev. Sci. Instrum. **72**, 3848 (2001).
[28] D. Townsend, M. Minitti, and A. G. Suits, Rev. Sci. Instrum. **74**, 2530 (2003).
[29] J. Lin, J. Zhou, W. Shiu, and K. Liu, Rev. Sci. Instrum. **74**, 2495 (2003).
[30] R. A. Morgan, A. Orr-Ewing, D. Ascenzi, M. N. R. Ashfold, W. J. Buma, C. R. Scheper, and C. A. de Lange, J. Chem. Phys. **105**, 2141 (1996).
[31] S. R. Ghandi and R. B. Bernstein, J. Chem. Phys. **87**, 6457 (1987).
[32] R. W. Anderson, J. Phys. Chem. A **101**, 7664 (1997).
[33] Y. Morino and T. Nakagawa, J. Mol. Spectrosc. **26**, 496 (1968).
[34] M. N. Daud, G. G. Balint-Kurti, and A. Brown, J. Chem. Phys. **74**, 54305 (2005).
[35] T. Suzuki (private communication).
[36] M. D. Morse, K. F. Freed, and Y. B. Band, J. Chem. Phys. **70**, 3604 (1979).